JOURNAL OF SOLID STATE CHEMISTRY 119, 324–330 (1995)

Preparation, Properties, and Crystal Structures of α- and β-$ScCrC_2$

Rainer Pöttgen, Anne M. Witte, Wolfgang Jeitschko,[1] and Thomas Ebel

Anorganisch-Chemisches Institut, Universität Münster, Wilhelm-Klemm-Strasse 8, D-48149 Münster, Germany

Received March 10, 1995

The new carbide $ScCrC_2$ crystallizes in two very closely related modifications. Their structures were determined from single-crystal X-ray data. The high-temperature (β) form has a small hexagonal cell, which corresponds to the subcell of the low-temperature (α) modification: $P6_3/mmc$, a = 323.7(1) pm, c = 914.9(3) pm, Z = 2, and R = 0.048 for 113 structure factors and 9 variable parameters. In the superstructure of α-$ScCrC_2$, both rotational and translational symmetry is lost: $Pmmn$, a = 324.34(3) pm, b = 915.02(3) pm, c = 561.48(4) pm, Z = 4, and R = 0.028 for 259 F-values and 22 variables. In the structure of β-$ScCrC_2$ the Sc and Cr positions correspond to the Ni and As positions of the NiAs structure and the trigonal prismatic voids formed by the Sc atoms are occupied by C_2 pairs with a C–C bond length of 160(1) pm. In α-$ScCrC_2$ one half of these C_2 pairs is contracted with a bond length of 142.6(7) pm; the other half of the carbon atoms has negligible C–C interactions (188(1) pm). The phase transition is discussed in terms of the "order–disorder" and the "soft-mode" models. The polyanion $(CrC_2^{3-})_n$ is two-dimensionally infinite and the Cr atoms obtain oxidation numbers of approximately +3. Compact, polycrystalline samples of α-$ScCrC_2$ are weakly paramagnetic and semiconducting.

INTRODUCTION

The binary system chromium–carbon is characterized by the three carbides Cr_3C_2 (1), Cr_7C_3 (2), and $Cr_{23}C_6$ (3). With the rare-earth elements and the actinoids several ternary chromium carbides were observed. The compounds $R_2Cr_2C_3$ (R = Y, Gd–Lu) with $Ho_2Cr_2C_3$-type structure (4, 5), $UCrC_2$ (6) and UCr_4C_4 (7) contain isolated carbon atoms, while isolated carbon atoms together with C_2 pairs occur in the carbides $U_2Cr_2C_5$ (8), $Th_2Cr_2C_5$ (9), and Sc_2CrC_3 (10). In the present paper, we report about two modifications of the new carbide $ScCrC_2$. The atomic positions of both forms are very similar, suggesting a displacive type phase transition. Nevertheless, the hexagonal high-temperature (β) form seems to be retained in quenched samples. At least such samples lack the long-range order, which manifests itself by the superstructure of the orthorhombic low-temperature (α) form. A preliminary account on this work was given earlier (11).

SAMPLE PREPARATION

Starting materials for the preparation of $ScCrC_2$ were filings of scandium metal (99.9%, Kelpin), chromium powder (150 mesh, 99.9%, Alpha), and graphite flakes (20 mesh, 99.5%, Alpha). Mixtures of the elemental components with the ideal composition were cold-pressed to pellets of about 300 mg and reacted in an arc-melting furnace under an argon atmosphere. The arc-melted buttons were subsequently wrapped in tantalum foil, enclosed in evacuated silica tubes, and annealed between 2 and 4 weeks at temperatures of 850 or 900°C. The reaction products were single-phase $ScCrC_2$ in the as-cast samples as well as in the annealed samples.

The structure determinations showed two very closely related modifications of $ScCrC_2$. The crystals of the high-temperature modification were isolated from the (rapidly cooled) arc-melted sample. The crystals of the low-temperature form were taken from a sample, which was obtained by annealing an arc-melted button in a high-frequency furnace. For this purpose the sample was placed in an evacuated, sealed silica tube, which was cooled on the outside by flowing water, to minimize the attack of the tube by the sample. The sample was briefly heated above the (not determined) melting point and subsequently annealed for 10 hr at about 100 K below that temperature. Thus, the phase transition from the high to the low temperature modification of $ScCrC_2$ must occur at a relatively high temperature.

CHEMICAL AND PHYSICAL PROPERTIES

Most properties of the two closely related modifications of $ScCrC_2$ are expected to be similar and the samples (of the α form) used for the chemical and most physical characterizations were taken from the buttons annealed at 900°C. $ScCrC_2$ crystallizes in the form of elongated prisms. They are of light-gray color with metallic luster. In contrast to the binary scandium carbides they are not

[1] To whom correspondence should be addressed.

0022-4596/95 $12.00

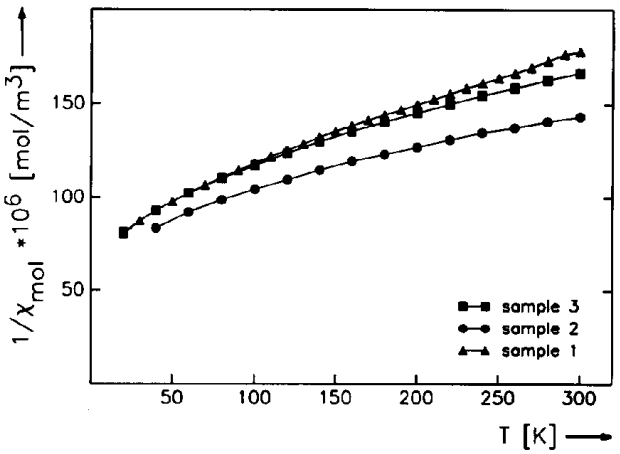

FIG. 1. Reciprocal magnetic susceptibility $1/\chi$ as a function of temperature of three different $ScCrC_2$ samples. Sample 1 was rapidly quenched after the arc-melting, the others were annealed at 850°C.

sensitive to air or moisture. Energy-dispersive X-ray fluorescence analyses did not reveal any impurity elements heavier than sodium.

The magnetic susceptibilities of three different polycrystalline samples were measured in a SQUID magnetometer in the temperature range from 20 to 300 K at magnetic flux densities of between 1 and 4 T. Sample 1 was rapidly cooled after the arc-melting and not annealed, while the other two samples were annealed for 20 days at 850°C. In spite of the differing heat-treatments the three samples show similar magnetic properties. As will be discussed further below, the high-temperature modification possibly contained microdomains with short-range order corresponding to the low-temperature form. The magnetic susceptibilities of all three samples were not field-dependent, indicating the absence of ferromagnetic impurities. Figure 1 shows plots of the inverse susceptibilities versus temperature of the three samples. It can be seen that all three samples show deviations from the linear behavior expected for the Curie–Weiss law. At best this law is approached at temperatures above 150 K for sample 1, which was quenched directly after the arc-melting. We have evaluated the data above 150 K according to the Curie–Weiss law. The magnetic moments varied between μ_{exp} = 1.5 (±0.1) μ_B per formula unit (f.u.) for sample 1 and μ_{exp} = 1.9 (±0.3) μ_B/f.u. for sample 2. We have also fitted all data points shown in Fig. 1 to the modified Curie–Weiss law $\chi = \chi_0 + C/(T - \Theta)$. These fits resulted in the temperature independent values of the magnetic susceptibilities χ_0 of between 2.5 (±0.2) × 10^{-9} m^3/f.u. (sample 1) and 4.4 (±0.2) × 10^{-9} m^3/f.u. (sample 2) with the considerably lower magnetic moments of μ_{exp} = 0.8 (±0.1) μ_B/f.u. for samples 2 and 3, and μ_{exp} = 0.9 (±0.1) μ_B/f.u. for sample 1.

The electrical conductivities of several different samples of α-$ScCrC_2$ were determined with a four-probe technique as described previously (12). The electrical resistivity behavior is that of a semiconductor, where the specific conductivity σ increases with increasing temperature. An activation energy of E_a = 0.05 (±0.01) eV was obtained by evaluation of the equation $\sigma = \sigma_0 \exp(E_a/2kT)$ for the steepest portion of the ρ ($=1/\sigma$) vs $1/T$ plot at high temperatures (Fig. 2). The results were completely reproducible. This small activation energy is most likely due to impurity levels and the intrinsic band gap may be much larger. Semiconducting behavior was also observed for the carbides $Sc_5Re_2C_7$ (13), $YbAl_3C_3$ (14), $ScT_{1-x}C_2$ (T = Fe, Co, Ni) (15), and $LnRhC_2$ (Ln = La, Ce) (16).

STRUCTURE DETERMINATIONS

The crystal structure of the low-temperature form was determined first. Single crystals were examined in a Weissenberg camera. They showed hexagonal symmetry, however, very weak superstructure reflections were found with the four-circle diffractometer. They violated the hexagonal symmetry and the full structure was found to be orthorhombic with cell dimensions corresponding to the orthorhombic setting of the hexagonal subcell.

The lattice constants of the orthorhombic cell were determined from the peak positions of 22 high angle reflections (48° < 2θ < 62°) measured on the four-circle diffractometer (Mo $K\alpha_1$: λ = 70.926 pm): a = 324.34(3) pm, b = 915.02(3) pm, c = 561.48(4) pm, and V = 0.16664 nm^3. The c/a ratio of 1.7311 of this cell is very close to the ideal value $\sqrt{3}$ = 1.7321 of the hexagonal subcell of α-$ScCrC_2$. This subcell is very pronounced: the strongest

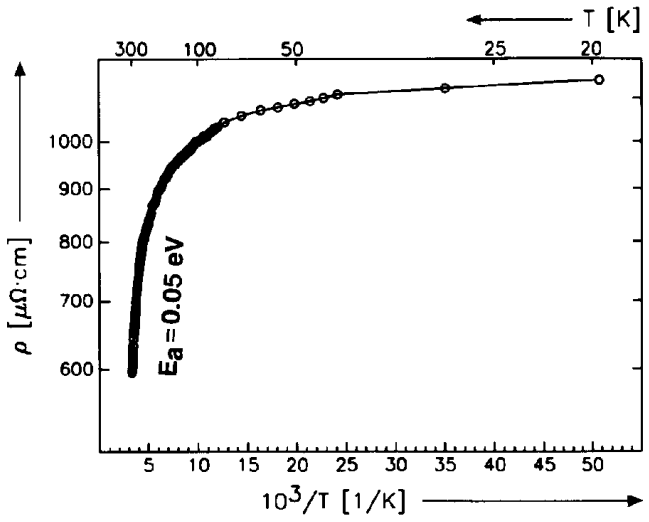

FIG. 2. Electrical resistivity of $ScCrC_2$ as a function of temperature. The activation energy E_a was calculated from the steepest portion of the ln ρ vs $1/T$ plot.

TABLE 1
Crystallographic Data for α- and β-$ScCrC_2$

	α-$ScCrC_2$		β-$ScCrC_2$
	Superstructure	Subcell	
Space group	*Pmmn* (No. 59)	$P6_3/mmc$ (No. 194)	$P6_3/mmc$ (No. 194)
Cell-constants (pm)[a]	a = 324.34(3)	a = 324.16(3)	a = 323.7(1)
	b = 915.0(1)	c = 915.0(1)	c = 914.9(3)
	c = 561.48(4)	c/a = 2.822	c/a = 2.826
Cell volume [nm^3]	V = 0.16663	V = 0.08332	V = 0.08302
Formula units per cell	Z = 4	Z = 2	Z = 2
Formula weight	120.97	120.97	120.97
Calculated density (g/cm^3)	q_{calc} = 4.82	q_{calc} = 4.82	q_{calc} = 4.82
Crystal size [μm^3]	22 × 22 × 130	22 × 22 × 130	22 × 44 × 66
Scan range (2θ)	80°	80°	90°
Range in *hkl*	±5, ±16, ±10	±2, ±4, ±16	±3, ±6, 0 − 18
Highest/lowest transmission	1.07	1.07	1.11
Total no. of reflections	4120	2006	1356
Data after averaging	649	142	280
Inner residual (on F-values)	R_i = 0.031	R_i = 0.027	R_i = 0.036
Reflections with $I > 3\sigma(I)$	259	98	113
Extinction corr. value, g[b]	$g = 1.4(1) \times 10^{-6}$	$g = 7(1) \times 10^{-6}$	$g = 1(1) \times 10^{-6}$
Number of variables	22	9	9
Conventional residual	R = 0.028	R = 0.038	R = 0.048
Weighted residual[c]	R_w = 0.028	R_w = 0.038	R_w = 0.048
Highest residual density [$e/Å^3$]	1.4	1.5	3.8

[a] The lattice constants of the subcell and of β-$ScCrC_2$ were determined from the Guinier powder data, and those of the α-superstructure from the four-circle diffractometer data.
[b] The extinction correction value g is defined by: corr.factor = $1/(1 + g \cdot I_c)$.
[c] Weights were according to $w = 1/\sigma(F)^2$ with $\sigma(F) = \sigma(F^2)/2F$ and $\sigma(F^2) = [\sigma(I)^2 + (0.02 \cdot F^2)^2]^{1/2}$.

reflection of the superstructure, calculated (17) with the data of the refined structure, had intensities of less than 1% of the strongest subcell reflections. The Guinier powder diagram showed only the subcell reflections. The lattice constants of this subcell were determined by least-squares fits of these data, recorded with Cu$K\alpha_1$ radiation using α-quartz (Riedel–de Haën, a = 491.30 pm, c = 540.46 pm) as an internal standard: a = 324.16(3) pm, c = 915.0(1) pm, and V = 0.08327 nm^3.

Single-crystal intensity data were recorded on an automated four-circle diffractometer with graphite-monochromated Mo $K\alpha$ radiation and a scintillation counter with pulse-height discriminator. The background was determined at both ends of each $\theta/2\theta$ scan, and an absorption correction was applied from psi scan data. Additional crystallographic data are summarized in Table 1. The systematic extinctions and the high Laue symmetry $6/mmm$ of the hexagonal subcell (*hhl* observed only with $l = 2n$) led to the space groups $P6_3/mmc$ $P\bar{6}2c$, and $P6_3mc$ of which the group with the highest symmetry $P6_3/mmc$ (no. 194) was found to be correct during the structure refinements. The positions of the metal atoms were determined from a Patterson synthesis, the carbon atoms were found by a difference Fourier analysis. The structure was refined by a full-matrix least-squares program using atomic scattering factors (18), corrected for anomalous dispersion (19).

The space group extinctions of the orthorhombic superstructure (*hk*0 observed only with $h + k = 2n$) led to the space groups $Pmmn$, $Pm2_1n$, and $P2_1mn$, of which the centrosymmetric group *Pmmn* (no. 59) was found to be correct during the final least-squares cycles. Thus, in going from the hexagonal group $P6_3/mmc$ to *Pmnm* (the corresponding nonstandard setting of *Pmmn*) we have lost both rotational and translational symmetry: the space group *Pmnm* is a *klassengleiche* subgroup of *Cmcm*, which in turn is a *translationengleiche* subgroup of $P6_3/mmc$ (20, 21). After transforming the positional parameters from the subcell setting $P6_3/mmc$ to the *Pmnm* setting of the superstructure (Fig. 3) followed by the transformation to the standard setting *Pmmn*, the structure refinement went smoothly to the residuals listed in Table 1. As a check for the composition the occupancy parameters were refined. No severe deviations from the ideal occupancies were found (Table 2), and in the final cycles the ideal occupancy values were assumed again.

For estimating the quality of the determination of the superstructure the overall residual (R = 0.028) is not a

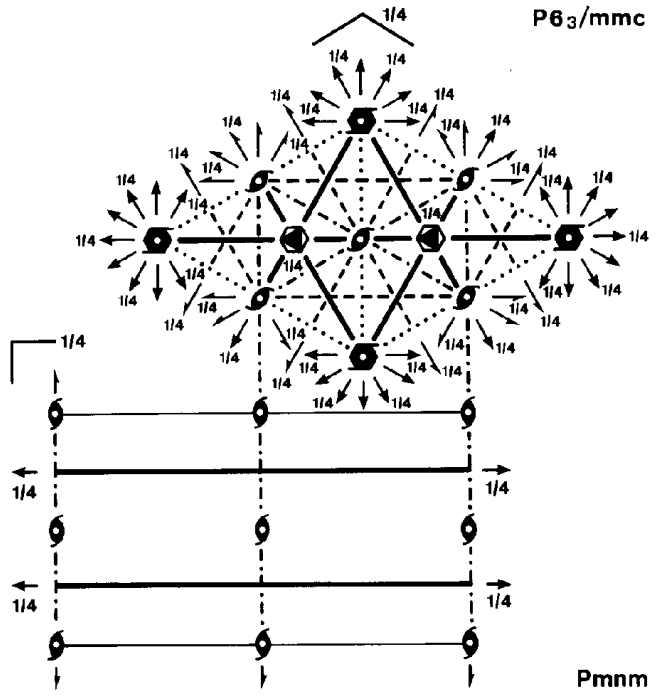

FIG. 3. Space group symmetries of the hexagonal β- and the orthorhombic α-modification of $ScCrC_2$. Note that the origin is different for the two cells.

reliable indicator, however, the residual for the 31 superstructure reflections with the 3σ cutoff of $R = 0.099$ is also reasonable. We also refined the structure with a 1σ cutoff. This refinement led to an overall residual of $R = 0.043$ for 353 structure factors and $R = 0.158$ for 103 superstructure reflections. For all of these refinements the positional and thermal parameters agreed within two combined standard deviations. The final positional parameters and interatomic distances are listed in Tables 2 and 3.

It was already mentioned above that the hexagonal subcell of α-$ScCrC_2$ is dominating. We thought that it might correspond to a potential high-temperature modification of this carbide. We therefore investigated a crystal of $ScCrC_2$, which was taken from a rapidly cooled arc-melted sample. It was mounted on the four-circle diffractometer and we searched in vain for superstructure reflections. A complete data set of this hexagonal crystal was collected and refined. The crystal data of this *b*-form of $ScCrC_2$ are also summarized in Tables 1–3. Listings of the structure factors for both modifications are available from the authors.

DISCUSSION

We will first discuss the structure of the hexagonal high-temperature β-form, which corresponds to the very pronounced subcell of the low-temperature α-modification. This cell contains only 8 atoms and may be regarded as a "filled-up" version of the NiAs structure, where the Sc and Cr atoms correspond to the positions of the Ni and As atoms, and the carbon atoms fill octahedral voids formed by both the Sc and the Cr atoms. A similar atomic arrangement was recently found for the carbide $GdRuC_2$ (23), however, in the inverse form, where the Gd atoms of $GdRuC_2$ correspond to the Cr atoms in $ScCrC_2$ and the Ru atoms take the place of the Sc atoms. The orthorhombic distortion of $GdRuC_2$ results from the orientation of the C_2 pairs, which are aligned perpendicular to the sixfold axis of the NiAs structure, while they are parallel to this axis in $ScCrC_2$.

Topologically the structure of β-$ScCrC_2$ is also closely related to the structures of TiAs (24), ReB_3 (25), Cr_2AlC (26), $ZrPt_2Al$ (27), and $LiNbO_2$ (28). All of these crystallize in the space group $P6_3/mmc$ with the C, Ti, B (two-thirds), Cr, Pt, and O atoms on the 4*f* position and the other atoms on twofold positions in such a way that the same stacking sequence of the close packed layers is obtained. Chemical bonding in these structures is different of course, and Parthé (29) recommended such structures to be designated as *isopointal*, while the term *isotypic* should be reserved for structures with similar chemical bonding. The structure of β-$ScCrC_2$ may also be described as a filled-up version of the four-layer neodymium structure with the stacking sequence ABAC, ABAC. In β-$ScCrC_2$ all octahedral voids of the metal atoms are filled with carbon atoms. Consequently the NiAs-type structure might also be regarded as an ordered neodymium structure, a correspondence, which to our knowledge has never been emphasized. The structure of β-$ScCrC_2$ is also closely related to the structures of $ScNbN_{1-x}$ (30) and $ScTaN_{1-x}$ (31). These structures have corresponding metal positions, however, the 4*f* positions are occupied only by less than 50% with nitrogen atoms.

The orthorhombic superstructure of α-$ScCrC_2$ (Fig. 4) can be rationalized by considering the chemical bonding of the carbon atoms. In the high-temperature form these atoms occur in pairs with a (real or average) C–C bond distance of 160 pm. This distance is greater than the typical single-bond distance of 154 pm in hydrocarbons. In the superstructure of the low-temperature form this degenerate situation is resolved by a new kind of Jahn–Teller distortion. While there is only one kind of carbon atom in the hexagonal form, the superstructure has two kinds. The C1 atoms have moved apart in the superstructure (C–C distance: 188 pm), while the C2 atoms form pairs with a bond distance of 143 pm. This distance is in between a double (134 pm) and a single C–C bond (154 pm), as is frequently observed for such carbides (32).

Two kinds of mechanism may be considered for the phase transition between the high- and the low-tempera-

TABLE 2
Atomic Parameters of α- and β-$ScCrC_2$[a]

Atom	Position	Occ.	x	y	z	B_{11}	B_{22}	B_{33}	B_{12}	B_{13}	B_{23}	B or B_{eq}
					Pmmn (α-$ScCrC_2$)							
Sc	4*e*	1.008(2)	1/4	0.0009(2)	0.7490(3)	0.35(2)	0.40(2)	0.28(2)	0	0	−0.01(2)	0.345(9)
Cr1	2*b*	0.979(4)	1/4	3/4	0.0720(2)	2.97(7)	0.26(3)	0.53(4)	0	0	0	1.25(2)
Cr2	2*a*	1.012(4)	1/4	1/4	0.4057(3)	0.41(3)	0.39(3)	1.58(5)	0	0	0	0.79(2)
C1	4*e*	1.14(2)	1/4	0.1475(8)	0.082(1)	—	—	—	—	—	—	1.5(1)
C2	4*e*	0.99(2)	1/4	0.6721(5)	0.4170(7)	—	—	—	—	—	—	0.17(5)
					$P6_3/mmc$ (subcell of α-$ScCrC_2$)							
Sc	2*a*	1.017(5)	0	0	0	0.31(2)	B_{11}	0.34(4)	B_{11}	0	0	0.32(1)
Cr	2*c*	0.995(5)	1/3	2/3	1/4	1.42(4)	B_{11}	0.33(3)	B_{11}	0	0	1.06(2)
C	4*f*	1.03(2)	1/3	2/3	0.6624(8)	0.7(1)	B_{11}	1.9(2)	B_{11}	0	0	1.11(8)
					$P6_3/mmc$ (β-$ScCrC_2$)							
Sc	2*a*	1.02(1)	0	0	0	0.27(3)	B_{11}	0.43(4)	B_{11}	0	0	0.32(1)
Cr	2*c*	0.99(4)	1/3	2/3	1/4	1.51(5)	B_{11}	0.24(4)	B_{11}	0	0	1.09(2)
C	4*f*	0.99(1)	1/3	2/3	0.6627(9)	0.5(1)	B_{11}	1.8(3)	B_{11}	0	0	0.94(9)

[a] Standard deviations in the positions of the least significant digits are given in parentheses throughout the paper. The positional parameters of both structures were standardized using the program STRUCTURE TIDY (22). The occupancy parameters occ. were varied in separate least-squares cycles along with the thermal parameters. In the final cycles the ideal occupancies were assumed. The thermal parameters are $\times 10^{-4}$ in units of pm^2.

ture form of $ScCrC_2$. One is the displacive type and the other is the order–disorder transition. They correspond to two different interpretations of the data for the high-temperature structure. In the order–disorder model the high-temperature structure has a random distribution of C_2 pairs with C–C distances of 143 and 188 pm. The phase

TABLE 3
Interatomic Distances in α- and β-$ScCrC_2$[a]

						β-$ScCrC_2$						
Sc:	6	C	238.9(5)	Cr:	6	C	203.2(3)	C:	1	C	160(1)	
	6	Cr	295.4(1)		6	Sc	295.4(1)		3	Cr	203.2(3)	
	6	Sc	323.7(1)		6	Cr	323.7(1)		3	Sc	238.9(5)	
						α-$ScCrC_2$						
Sc:	1	C1	230.3(7)	Cr1:	4	C1	206.4(4)	C1:	1	C1	188(1)	
	2	C1	231.8(5)		2	C2	206.5(4)		1	Cr2	204.4(7)	
	2	C2	244.0(4)		2	Sc	292.6(2)		2	Cr1	206.4(4)	
	1	C2	244.5(5)		4	Sc	297.2(2)		1	Sc	230.3(7)	
	1	Cr1	292.6(2)		2	Cr2	313.4(2)		2	Sc	231.8(5)	
	2	Cr2	294.2(2)		2	Cr1	324.3(1)	C2:	1	C2	142.6(7)	
	2	Cr1	297.2(2)		2	Cr2	335.1(2)		2	Cr2	203.2(3)	
	1	Cr2	298.5(2)	Cr2:	4	C2	203.2(3)		1	Cr1	206.5(4)	
	2	Sc	323.3(2)		2	C1	204.4(7)		2	Sc	244.0(4)	
	2	Sc	324.3(1)		4	Sc	294.2(2)		1	Sc	244.5(5)	
	2	Sc	325.2(2)		2	Sc	298.5(2)					
					2	Cr1	313.4(2)					
					2	Cr2	324.3(1)					
					2	Cr1	335.1(2)					

[a] All distances shorter than 433 pm (Sc–Sc, Sc–Cr, Cr–Cr), 353 pm (Sc–C, Cr–C), and 324 pm (C–C) are listed.

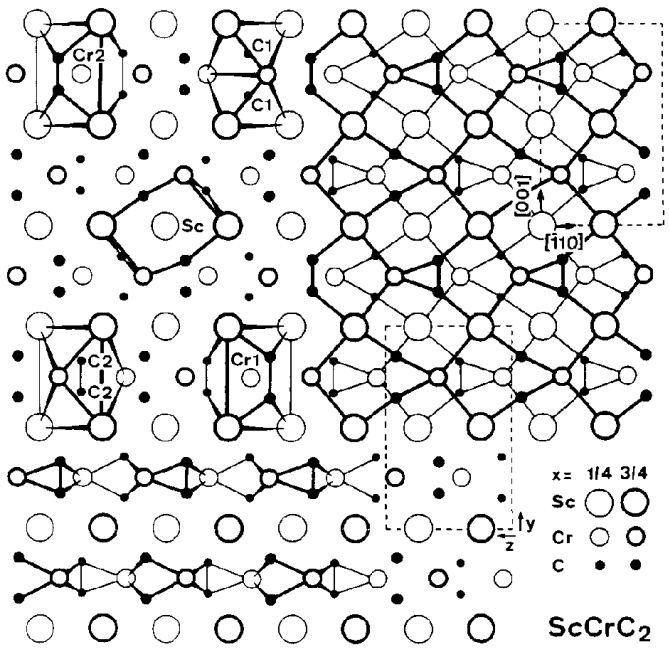

FIG. 4. Crystal structure and coordination polyhedra of α-$ScCrC_2$. Atoms connected by thick (at x = 3/4) and thin lines (x = 1/4) in the upper right-hand part of the drawing are situated on mirror planes, which extend perpendicular to the projection direction. In the lower left-hand part the two-dimensionally infinite $(CrC_2^{3-})_n$ polyanions are emphasized. Carbon pairs connected by a line have a bond distance of 142.6 pm; nonconnected carbon pairs have a C–C distance of 188 pm. In the hexagonal high-temperature (β) form (with the hexagonal cell in the upper right-hand corner) these carbon pairs are equivalent with a bond distance of 160 pm.

transition occurs when the long-range order sets in. In the other model, the soft-mode model (33), one assumes that at high temperatures the thermal motions of all atoms are great enough to stabilize the average structure with equal C–C distances of around 160 pm. The anisotropic thermal motions of the atoms have the greatest amplitudes in those directions, where they settle in the low-temperature form. That model is called the soft-mode model because the large thermal amplitudes correspond to a lattice mode of low frequency. Upon cooling the amplitudes increase and the frequency decreases until, at the phase transition, the atoms lock in at an extreme position. In both kinds of models one expects to find twin domains in the low-temperature form, which together mimic the higher symmetry (21).

Most likely for $ScCrC_2$ neither one of these models apply in their pure forms. In ceramic materials with soft-mode phase transitions, e.g., $Gd_2(MoO_4)_3$ (34, 35), long-range order is usually easily established. In fact, it is frequently impossible to retain the high-temperature form at room temperature by quenching. On the other hand, in compounds with order–disorder transitions, which frequently occur in intermetallics, e.g., in Cu_3Au, it is very easy to quench the high-temperature form. Normally for such compounds it is necessary to establish long-range order by annealing below the transition temperature. Thus the fact that the disordered high-temperature form of $ScCrC_2$ was retained by quenching favors the order–disorder model. On the other hand, only small atomic displacements are necessary to obtain the low-temperature form of $ScCrC_2$ from the high-temperature form, and this suggests that at temperatures just below the melting point, a dynamic model might be right. Possibly the high-temperature form contains many microdomains with short-range order and rapidly moving, fluctuating domain walls. In quenching, these randomly oriented microdomains are frozen in. This might explain why the positional and the anisotropic displacement parameters of β-$ScCrC_2$ and the hexagonal subcell of the α-form are practically the same (Table 2).

The anisotropic displacement parameters of the chromium atoms in α-$ScCrC_2$ are also of interest. The B_{11} value of the Cr1 atoms and the B_{33} value of the Cr2 atoms are rather large with about 3.0 and 1.6 Å^2 ($=10^{-4}$ nm^2), respectively. These parameters correspond to the rather large $B_{11} = B_{22}$ values of the only chromium position in the β-form (and the subcell of α-$ScCrC_2$). This might indicate that the low-temperature form is not fully ordered, or (more likely) the crystal used for the structure determination of the low-temperature form contained domains of the other two twin orientations. In any case it is worth mentioning, that these large displacements of the chromium atoms point in the direction of those C_2 pairs (the C1 atoms), which have moved apart in the low-temperature form (Fig. 5) and thus they have emptied some space, which can be occupied by the chromium atoms.

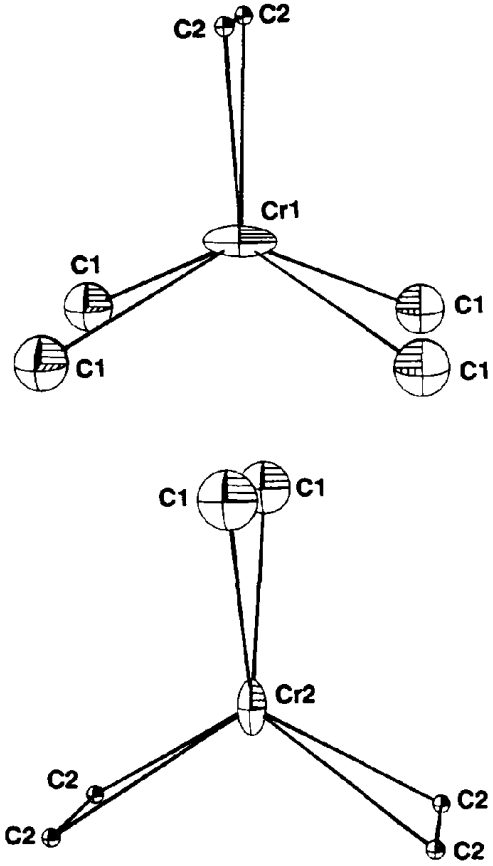

FIG. 5. Displacement parameters of the chromium and carbon atoms in α-$ScCrC_2$. The largest displacements (drawn at the probability limit of 80%) point toward the space between the C1 atoms.

The possible presence of the other twin domains was not taken into account when the structure of α-$ScCrC_2$ was refined from the X-ray data. In other words, the subcell reflections may be somewhat too strong as compared to the superstructure reflections. Therefore the displacements of all atoms in the α-form as compared to the β-form may actually be greater than the results of the least-squares refinements indicate, i.e. the C1–C1 distance may in reality be greater than 188 pm and the real C2–C2 distance may be shorter than 142.6 pm.

The rationalization of the chemical bonding and of the physical properties of $ScCrC_2$ is not straightforward. Certainly the bonding between the scandium atoms on the one hand and the chromium and carbon atoms on the other hand is predominantly ionic, while the bonding within the $(CrC_2^{3-})_n$ polyanion is primarily covalent. In aiming for integer oxidation numbers (formal charges) and in therefore counting the bond between the C2 atoms of 142.6 pm in the α-form as a double bond, one obtains the formula $(Sc^{3+})_2(Cr1^{3+})(Cr2^{3+})(C1^{4-})_2(C2_2)^{4-}$. Thus, the chromium

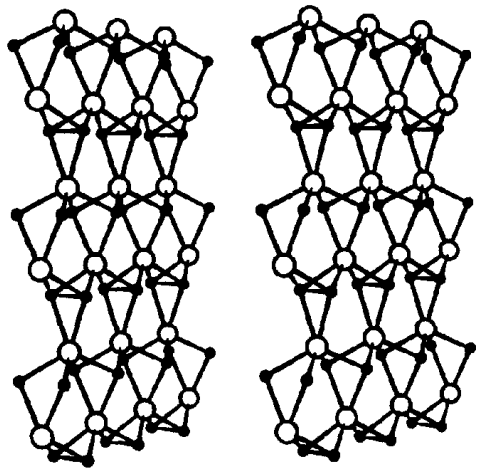

FIG. 6. Stereoplot of the two-dimensionally infinite polyanion in the structure of α-$ScCrC_2$.

atoms have an oxidation number of approximately +3. The $(CrC_2^{3-})_n$ polyanion is two-dimensionally infinite (Fig. 6). It consists of a close-packed layer of chromium atoms. These chromium atoms are held together by C_2 pairs, which have their axes oriented perpendicular to the layers. The Cr–Cr distances within the layers vary between 313 pm and 335 pm. These distances might still be considered as bonding distances. Nevertheless, the polyanion seems to be electronically unsaturated as is indicated by the weak paramagnetism, which corresponds approximately to two unpaired spins for the four chromium atoms per cell of the orthorhombic α-form.

The $(CrC_2^{3-})_n$ polyanionic layers are separated from each other by close-packed layers of scandium atoms. These scandium layers, together with the adjacent carbon atoms, have an arrangement which is known from the NaCl-type structure of ScC_{1-x} (36, 37). Thus, the scandium atoms are surrounded by six carbon atoms in octahedral arrangement. In addition to the carbon atoms the scandium atoms have six chromium neighbors at distances of between 292.6 pm and 298.5 pm. Some bonding character might also be ascribed to these interactions.

ACKNOWLEDGMENTS

We thank Dipl.-Ing. U. Rodewald and Dr. M. H. Möller for the collection of the four-circle diffractometer data, Dipl.-Chem. C. B. H. Evers for the electrical conductivity measurements, Mrs. U. Göcke for her help with the drawings, Mr. K. Wagner for the work at the scanning electron microscope, and Mr. C. Brendel for the differential scanning calorimetry measurements at an early stage of this work. Dr. G. Höfer (Heraeus Quarzschmelze) supported our work by a generous gift of silica tubes. We also acknowledge the Stiftung Stipendienfonds des Verbandes der Chemischen Industrie for a stipend to R.P. This work was supported by the Deutsche Forschungsgemeinschaft and the Fonds der Chemischen Industrie.

REFERENCES

1. S. Rundqvist and G. Runnsjö, *Acta Chem. Scand.* **23,** 1191 (1969).
2. A. Rouault, P. Herpin, and R. Fruchart, *Ann. Chim. (Paris)* **5,** 461 (1970).
3. A. L. Bowman, G. P. Arnold, E. K. Storms, and N. G. Nereson, *Acta Crystallogr. Sect. B* **28,** 3102 (1972).
4. W. Jeitschko and R. K. Behrens, *Z. Metallkd.* **77,** 788 (1986).
5. K. Zeppenfeld, R. Pöttgen, M. Reehuis, W. Jeitschko, and R. K. Behrens, *J. Phys. Chem. Solids* **54,** 257 (1993).
6. D. T. Cromer, A. C. Larson, and R. B. Roof, Jr., *Acta Crystallogr.* **17,** 272 (1964).
7. R. K. Behrens and W. Jeitschko, *Monatsh. Chem.* **118,** 43 (1987).
8. R. K. Behrens and W. Jeitschko, *Z. Kristallogr.* **182,** 19 (1988).
9. G. E. Kahnert, G. Block, R. K. Behrens, and W. Jeitschko, *Z. Kristallogr.* **186,** 154 (1989).
10. A. O. Pecharskaya, E. P. Marusin, O. I. Bodak, and M. D. Mazus, *Sov. Phys. Crystallogr. Engl. Transl.* **35,** 25 (1990).
11. R. Pöttgen and W. Jeitschko, *Z. Kristallogr. Suppl.* **7,** 153 (1993).
12. R. Pöttgen, W. Jeitschko, C. B. H. Evers, and M. A. Moss, *J. Alloys Compd.* **186,** 223 (1992).
13. R. Pöttgen and W. Jeitschko, *Z. Naturforsch, B. Anorg. Chem., Org. Chem.* **47,** 358 (1992).
14. Th. M. Gesing, R. Pöttgen, W. Jeitschko, and U. Wortmann, *J. Alloys Compd.* **186,** 321 (1992).
15. R. Pöttgen, W. Jeitschko, U. Wortmann, and M. E. Danebrock, *J. Mater. Chem.* **2,** 633 (1992).
16. R.-D. Hoffmann, W. Jeitschko, and L. Boonk, *Chem. Mater.* **1,** 580 (1989).
17. K. Yvon, W. Jeitschko, and E. Parthé, *J. Appl. Crystallogr.* **10,** 73 (1977).
18. D. T. Cromer and J. B. Mann, *Acta Crystallogr. Sect. A* **24,** 321 (1968).
19. D. T. Cromer and D. Liberman, *J. Chem. Phys.* **53,** 1891 (1970).
20. T. Hahn (ed.), "International Tables for Crystallography" Reidel, Dordrecht, 1983.
21. H. Wondratschek and W. Jeitschko, *Acta Crystallogr. Sect. A* **32,** 664 (1976).
22. L. M. Gelato and E. Parthé, *J. Appl. Crystallogr.* **20,** 139 (1987).
23. R.-D. Hoffmann and W. Jeitschko, *Z. Kristallogr.* **186,** 133 (1989).
24. K. Łukaszewicz and W. Trzebiatowski, *Bull. Acad. Pol. Sci. Cl. 3.* **2,** 277 (1954).
25. B. Aronson, E. Stenberg, and J. Åselius, *Acta Chem. Scand.* **14,** 733 (1960).
26. W. Jeitschko, H. Nowotny, and F. Benesovsky, *Monatsh. Chem.* **94,** 672 (1963).
27. R. Ferro, R. Marazza, G. Rambaldi, and A. Saccone, *J. Less-Common Met.* **40,** 251 (1975).
28. G. Meyer and R. Hoppe, *J. Less-Common Met.* **46,** 55 (1976).
29. E. Parthé, "Elements of Inorganic Structural Chemistry." Parthé, Geneva, 1990.
30. W. Lengauer, *J. Solid State Chem.* **82,** 186 (1989).
31. W. Lengauer and P. Ettmayer, *J. Less-Common Met.* **141,** 157 (1988).
32. W. Jeitschko, M. H. Gerss, R.-D. Hoffmann, and S. Lee, *J. Less-Common Met.* **156,** 397 (1989).
33. W. Cochran, *Adv. Phys.* **18,** 157 (1969).
34. W. Jeitschko, *Acta Crystallogr. Sect. B* **28,** 60 (1972).
35. B. Dorner, J. D. Axe, and G. Shirane, *Phys. Rev. B. Condens. Matter* **6**(5), 1950 (1972).
36. H. Nowotny and H. Auer-Welsbach, *Monatsh. Chem.* **92,** 789 (1961).
37. H. Rassaerts, H. Nowotny, G. Vinek, and F. Benesovsky, *Monatsh. Chem.* **98,** 460 (1967).